AD-A280 264

JMENTATION PAGE

1. AGENCY USE ONLY (Leave blank)	2. REPORT DATE	3. REPORT TYPE AND DATES COVERED
		FINAL/01 DEC 89 TO 31 DEC 93

4. TITLE AND SUBTITLE
SIMULATION OF MANUFACTURING PROCESSES

5. FUNDING NUMBERS
2304/A3
AFOSR-90-0094

6. AUTHOR(S)
C. A. HALL AND T. A. PORSCHING

7. PERFORMING ORGANIZATION NAME(S) AND ADDRESS(ES)
UNIVERSITY OF PITTSBURGH
OFFICE OF RESEARCH
350 THACKERAY HALL
PITTSBURGH PA 15260

8. PERFORMING ORGANIZATION REPORT NUMBER
AFOSR-TR- 94 0351

9. SPONSORING/MONITORING AGENCY NAME(S) AND ADDRESS(ES)
AFOSR/NM
110 DUNCAN AVE, SUTE B115
BOLLING AFB DC 20332-0001

10. SPONSORING/MONITORING AGENCY REPORT NUMBER
AFOSR-90-0094

DTIC ELECTE JUN 15 1994 S B D

11. SUPPLEMENTARY NOTES

12a. DISTRIBUTION/AVAILABILITY STATEMENT

APPROVED FOR PUBLIC RELEASE: DISTRIBUTION IS UNLIMITED

12b. DISTRIBUTION CODE

13. ABSTRACT (Maximum 200 words)

This report summarizes research surrounding the simulations of two manufacturing processes-the finishing and/or repair of material surfaces and the stamping of sheet metal parts.

Regarding the surface finishing project, a unified mathematical theory for the process of material removal by abrasion (grinding and polishing) was developed. Then strategies were formulated for material removal by Operator controlled (OC) or Computer Numerically Controlled (CNC) machines.

For the sheet metal stamping project, certain asymmetric numerical solution were characterized as symmetry breaking bifurcations of the differential algebraic equations (DAE) which mathematically describe the physical phenomena of sheet metal stretching. That is, these asymmetries are inherent in the mathematical rather than the numerical formulation of the problem.

14. SUBJECT TERMS

15. NUMBER OF PAGES

DTIC QUALITY INSPECTED 2

17. SECURITY CLASSIFICATION OF REPORT	18. SECURITY CLASSIFICATION OF THIS PAGE	19. SECURITY CLASSIFICATION OF ABSTRACT	20. LIMITATION OF ABSTRACT
UNCLASSIFIED	UNCLASSIFIED	UNCLASSIFIED	SAR(SAME AS REPORT)

NSN 7540-01-280-5500

FINAL TECHNICAL REPORT
AIR FORCE OFFICE
OF
SCIENTIFIC RESEARCH
GRANT AFOSR-90-0094

DECEMBER, 1989—DECEMBER, 1993

SIMULATION OF
MANUFACTURING PROCESSES

PRINCIPAL INVESTIGATORS
C. A. HALL AND T. A. PORSCHING

INVESTIGATOR
P. J. RABIER

Department of Mathematics and Statistics
University of Pittsburgh
Pittsburgh, PA 15260

May 1994

ABSTRACT. This report summarizes research surrounding the simulation of two manufacturing processes—the finishing and/or repair of material surfaces and the stamping of sheet metal parts.

Regarding the surface finishing project, a unified mathematical theory for the process of material removal by abrasion (grinding and polishing) was developed. Then strategies were formulated for material removal by Operator Controlled (OC) or Computer Numerically Controlled (CNC) machines.

For the sheet metal stamping project, certain asymmetric numerical solutions were characterized as symmetry breaking bifurcations of the differential algebraic equations (DAE) which mathematically describe the physical phenomena of sheet metal stretching. That is, these asymmetries are inherent in the mathematical rather than the numerical formulation of the problem.

CONTENTS

1. Introduction.

There were two major projects comprising this research program on simulation of manufacturing processes. The first involves the finishing and/or repair of material surfaces and the second the stamping of sheet metal parts.

Objectives of the surface finishing project were to develop a unified mathematical theory for the process of material removal by abrasion (grinding and polishing), and then to synthesize a strategy for material removal by a an Operator Controlled (OC) machine or a Computer Numerically Controlled (CNC) machine that will accurately approximate a desired removal profile. Of particular interest were computer simulations of (i) the fabrication of large optics (lenses and mirrors) of the type used in telescopes (such as the Hubble space telescope) and cinetheodolites, and (ii) the reclamation of damaged aircraft canopies. In pursuit of these objectives a model for the kinematics of a Draper polishing machine was developed and experiments to test this model were designed in cooperation with Contraves-Goerz Corporation. Also, computational experiments were continued on the use of mollifers or smoothing functions to achieve a desired material removal.

The motivation for the sheet metal stamping project was based on an observation made a few years ago concerning the numerical solutions of sheet metal punch problems. Even though the problems were mathematically symmetric, the numerical solutions produced would typically be grossly asymmetric. This was explained at the time as a "lack of robustness" of the numerical methods. Under this research project, we attempted to characterize these anomolies as symmetry breaking bifurcations of the DAE (differential algebraic equations) which mathematically describe the physical phenomena of sheet metal stretching. That is, our thesis was that these asymmetries are inherent to the mathematical (rather than the numerical) formulation.

2. Surface Finishing. OC and CNC surface finishing machines have been used in the optical industry for more than twenty years. See for example [1-11]. More recently, this technology has also been applied to the restoration of aircraft canopy transparencies [12]. While some of the modeling principles and approximations underlying the control of surface finishing machines have appeared in the open literature ([1-3], [5]. [7], [9], [11], [13]), a comprehensive mathematical approach to the overall problem did not exist in the public domain prior to 1990. This is not surprising in view of the complex physics and general geometrical considerations that influence surface finishing processes. Nevertheless, certain common threads ran through the published literature on the subject, and in the series of papers [14-16], and especially [17] we fashioned these into a systematic, unified mathematical treatment of the problem.

One of the essential ingredients in any mathematical approach to a finishing process is the determination of a *material removal rate* corresponding to a given machine tool configuration. This is the rate at which material is removed at each point on the workpiece by abrasion due to the relative motion of the workpiece and the tool. By a tool we shall mean a device whose contact region with the workpiece is a homogeneous, time invariant lamina. Thus, although the physical tool may be quite complex, involving possibly a series of cranks, levers and other drive mechanisms, the mathematical model involves a relatively simple two-dimensional entity whose kinematical nature is reasonably well understood. Of course, in determining the motion of any specific tool we must incorporate the effects of

its constitutive parts. However, one of the consequences of our analysis is that for a class of tools that are widely used in practice (the so-called freely pinned tools) it suffices to know only the motion of a single point on the lamina (its mass center). The solution of this latter problem is theoretically a straightforward (though perhaps tedious) exercise in plane mechanics. In [17] we presented the kinematics surrounding a general removal rate, gave its definition, and illustrated the idea with an example.

The second main item in our theory is the *material removal profile* that the machine produces. This is the amount of material removed at each point on the workpiece by the machine. The material removal profile can be synthesized from a knowledge of the removal rate and the *dwell times* associated with points on the workpiece. If all of the relative motion between the tool and workpiece is accounted for in the removal rate, then the material removal profile at a given point on the workpiece is just the sum of the individual removal contributions made by points on the tool contacting the given point over the duration of the finishing process. However, for modern CNC machines it is also useful to develop the removal rate in terms of a restricted set of motions called *local motions*. In this case the removal rate is described relative to a reference frame whose origin is referred to as the *tool center*. The removal profile is then produced by allowing the tool center to move along a path on the workpiece according to some speed distribution. The motions of the tool center are what we call *global motions*. If the speeds of the global motions are small relative to those of the local motions (which is usually the case), then one can neglect their contribution to the removal rate, and the removal profile assumes the form of a convolution integral. We developed this idea in detail in [17].

The third subject in the formulation of a mathematical theory for finishing is the determination of a machine *material removal strategy*. This amounts to the selection of a set of admissible machine controls so as to achieve a specified pattern of material removal from the workpiece. For OC machines such a strategy ususally involves the determination of an optimal set of dwell times, or the choice of an optimal path and/or speed distribution for the tool center. In [17] we showed how to utilize the notion of a *mollifier* along with numerical quadrature rules to produce a path-speed strategy. Although this strategy is in general suboptimal, the bounds that we derived for the error produced by it show that in theory it can be made as precise as one wishes by proper adjustment of machine parameters.

We now discuss some of these ideas in more detail. Assume that the interface between the tool and workpiece motions is confined to a fundamental plane. In this plane we fix a frame of reference F with origin O. To describe the relative motion between points at the tool-workpiece interface we denote the region of contact at any time by G. Frequently, G is the region contacted by an abrasive pad so that we also refer to G as the tool pad. Although the motion of the workpiece can be built into that of G, it is more natural to treat this explicitly. However, we limit the workpiece motion to pure rotations about O with angular velocity Ω. This is in keeping with the type of OC polishing machines that have been traditionally used to finish an important class of optical surfaces, the so-called axisymmetric surfaces [3], [13].

Let $P \in G$ have the time dependent position vector $\mathbf{P}(t)$, where t is time, and let $\mathbf{q}$ be the relative velocity between P and the workpiece. If we represent $\mathbf{q}$ as a complex number,

then we have shown [17] that

$$\mathbf{q} = [\dot{\sigma} + i\sigma(\dot{\beta} - \Omega)]e^{i\beta} + i\rho(\omega - \Omega)e^{i(\alpha+\beta)}, \tag{1}$$

where σ and β are the polar coordinates of C, the mass center of G relative to the frame F, ρ and α are the polar coordinates of P relative to a line through O and C, and ω is the angular velocity of G in the frame F.

Using the representation (1), we have proven that in the special. but important, case in which the tool pad G is free to rotate about a smooth pin through C (a freely pinned tool), the relative velocity $\mathbf{q}$ is the same at all points of G providing that its initial angular velocity is zero. This is of great importance in computer simulations of finishing processes since it implies that in order to determine the material removal rate at a given point on the workpiece, it suffices to keep track only of the relative velocity of C and whether or not the point is contacted by G.

Now we turn to the definition of the material removal rate. Preston's hypothesis [18] provides a viable (and widely used) description of material removal by abrasion. This states that the rate at which material is removed from the workpiece by the tool is proportional to the product of the pressure and relative speed between the tool and workpiece. The constant of proportionality depends on the interface pressure, the workpiece material, the tool pad material, and any additional agents such as slurries or lubricants that have been used to enhance or retard the abrasiveness of the pad.

To define the *instantaneous material removal rate* it is convenient to use a reference frame F' fixed on the workpiece, i.e., rotating with it. In this frame the relationship between the relative velocity $\mathbf{q}'$ of a point $P \in G$ and $\mathbf{q}$ is simply $\mathbf{q}' = \mathbf{q}e^{-i\xi}$, where the angle ξ satisfies the condition $\dot{\xi} = \Omega$.

Let the point Y on the workpiece have position vector $\mathbf{y}$ which, since we are using the frame F', does not depend on t. If $\Phi(\mathbf{y}, t)$ denotes the instantaneous material removal rate at the point Y at time t, then according to Preston's hypothesis, either $\Phi(\mathbf{y}, t) = 0$ or

$$\Phi(\mathbf{y}, t) = K^* p|\mathbf{q}'| = K^* p|\mathbf{q}|. \tag{2}$$

where P is the point on G that contacts Y at time t and $\mathbf{q}$ is given by (1). In (2) K^* is the proportionality constant, and p is the pressure.

A second and perhaps more useful type of removal rate is obtained by eliminating the explicit dependence of the removal rate on t. Thus, in addition to Φ, we consider the *average material removal rate*

$$\phi(\mathbf{y}) \equiv \frac{1}{T_1 - T_0} \int_{T_0}^{T_1} \Phi(\mathbf{y}, t)dt, \tag{3}$$

where $[T_0, T_1]$ is some appropriately chosen time interval.

The complex kinematical relationships of most surface fininshing machines preclude the representation of their average removal rates in closed form. Consequently, we use numerical quadrature to generate them.

If we take $T_0 = 0, T_1 = t$, suppress the dependence on y, and emphasize the dependence on t, we can write (3) as

$$\phi(t) = \frac{1}{t}\int_0^t \Phi(s)ds. \tag{4}$$

We are interested in the calculation of $\phi(t)$ for large values of t. For this purpose we differentiate (4) to get

$$\frac{d}{dt}(t\phi) = \Phi(t), \tag{5}$$

and note that by (4), we also have

$$\phi(0) = \Phi(0). \tag{6}$$

Relations (5) - (6) constitute an initial value problem for $\phi(t)$. We solve this numerically by using the midpoint method. We let $t_0 = 0,\ t_{n+1} = t_n + h,\ n = 0.1.....$ If ϕ_n denotes the approximate value of $\phi(t_n)$, then the midpoint method yields

$$\phi_{n+1} = \frac{t_n\phi_n + h\Phi_{n+1/2}}{t_{n+1}},\ n = 0, 1, \dots, \tag{7}$$

where $\Phi_{n+1/2} = \Phi(t_n + h/2)$ and $\phi_0 = \Phi(0)$. Note that an any finite interval $[0, T]$, we have

$$\phi_n = \phi(t_n) + O(h^2),$$

i.e., the method is second order. Note further that (7) can also be written as

$$\phi_{n+1} = \frac{n}{n+1}\phi_n + \frac{1}{n+1}\Phi_{n+1/2}. \tag{8}$$

We now consider the calculation of

$$\Phi_{n+1/2} = \Phi(\mathbf{y}, t_n + h/2), \tag{9}$$

where Φ is given by (2). Equation (9) holds provided that at time t the point P on the pad whose representation in the frame F is

$$P = \sigma e^{i\beta} + \rho e^{i(\alpha+\beta)} \tag{10}$$

coincides with the given point y.

In the frame F' let $\mathbf{y} = re^{i\theta}$ where r and θ do not depend on t. See Figure 1. Since in F'

$$P = [\sigma e^{i\beta} + \rho e^{i(\alpha+\beta)}]e^{-i\Omega t},$$

the constraint $P = \mathbf{y}$ becomes

$$\sigma e^{i\beta} + \rho e^{i(\alpha+\beta)} = re^{i(\theta+\Omega t)}. \tag{11}$$

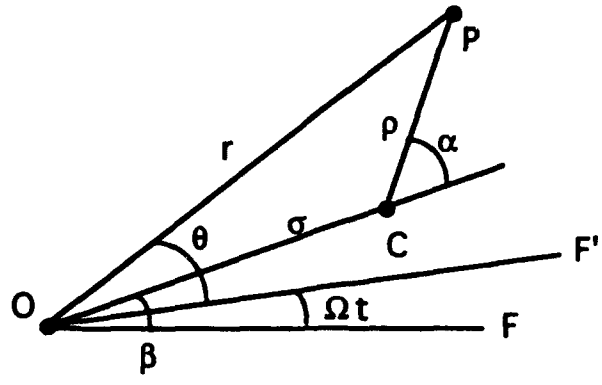

Figure 1. The Frames F and F'.

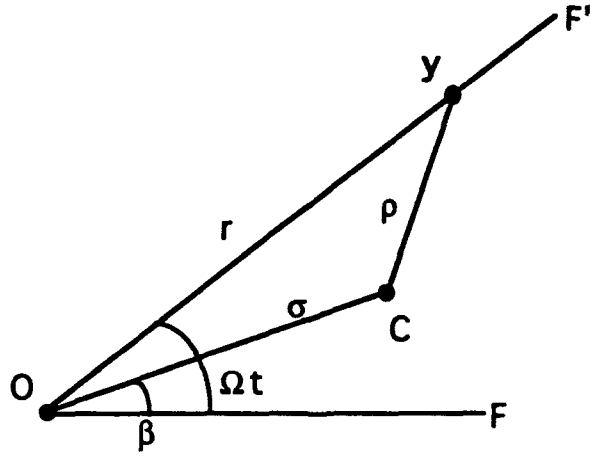

Figure 2. The constraint (12).

If (11) does not hold then in place of (9) we have

$$\Phi(\mathbf{y}, t) = 0.$$

We assume that t is large enough so that $\phi(\mathbf{y}, t)$ is axi-symmetric. This allows us to fix θ at some convenient value, say $\theta = 0$. We also assume that the pad G is the disk $0 \leq \rho \leq s$. Then in view of Figure 2 condition (11) holds if and only if

$$r^2 + \sigma^2 - 2r\sigma\cos(\Omega t - \beta) \leq s^2. \tag{12}$$

As an illustration of these ideas, we apply this general theory to develop the form of the material removal rates produced by a Draper polishing machine, an OC machine that is used in the finishing of axisymmetric optical surfaces. Figure 3 is a schematic of a typical Draper machine. The workpiece is mounted on a circular bed that rotates with constant (but adjustable) angular velocity Ω about its center O. The tool consists of a circular abrasive pad G that is freely pinned at C to a beam PQ. (Some machines also allow forced rotation of the pad G about C.) The beam is free to slide in a collar at Q and is driven in a reciprocal manner by a crank arm that rotates with constant angular velocity λ. The other parameters of the machine are the lengths $A, B. R, T$, as well as S, the distance of the pin C from P, the length of the crank arm a, and s, the radius of the pad.

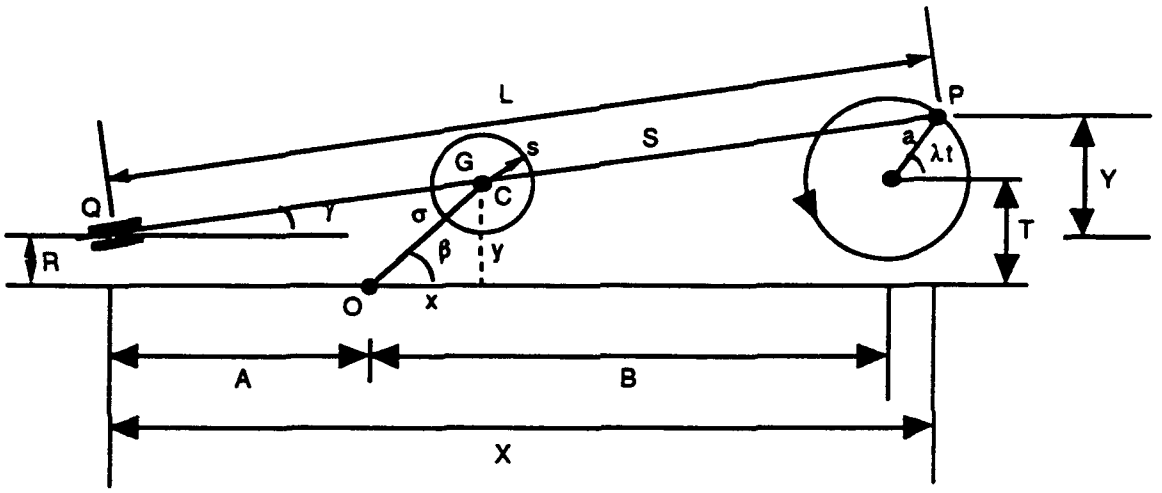

Figure 3. Schematic of a Draper machine.

Since the pad is freely pinned, $\omega = \Omega$ and so (1) reduces to

$$\mathbf{q} = [\dot{\sigma} + i\sigma(\dot{\beta} - \Omega)]e^{i\beta}. \tag{13}$$

Therefore, it suffices to determine σ and β as functions of the lengths a, A, B, R, S, T and the angular velocity λ. But by Figure 3,

$$\sigma \cos\beta = B + a\cos\lambda t - S\cos\gamma \equiv x,$$
$$\sigma \sin\beta = T + a\sin\lambda t - S\sin\gamma \equiv y.$$

The angle γ is defined by the conditions,

$$L\cos\gamma = A + B + a\cos\lambda t \equiv X,$$
$$L\sin\gamma = T - R + a\sin\lambda t \equiv Y.$$

We then have

$$\cos\gamma = \frac{X}{\sqrt{X^2 + Y^2}},$$
$$\sin\gamma = \frac{Y}{\sqrt{X^2 + Y^2}},$$

and similarly

$$\cos\beta = \frac{x}{\sigma},$$
$$\sin\beta = \frac{y}{\sigma},$$

where

$$\sigma = \sqrt{x^2 + y^2}.$$

Finally, for use in (13) we have

$$\dot{\sigma} = \frac{x\dot{x} + y\dot{y}}{\sigma},$$
$$\dot{x} = -a\lambda \sin\lambda t - S\frac{d}{dt}(\cos\gamma),$$
$$\dot{y} = a\lambda \cos\lambda t - S\frac{d}{dt}(\sin\gamma),$$
$$\frac{d}{dt}(\cos\gamma) = \frac{Y^2\dot{X} - XY\dot{Y}}{(X^2+Y^2)^{3/2}},$$
$$\frac{d}{dt}(\sin\gamma) = \frac{X^2\dot{Y} - XY\dot{X}}{(X^2+Y^2)^{3/2}},$$
$$\dot{X} = -a\lambda \sin\lambda t,$$
$$\dot{Y} = a\lambda \cos\lambda t,$$
$$\dot{\beta} = \frac{\sigma\dot{y} - y\dot{\sigma}}{\sigma^2\cos\beta}.$$

Figure 4 shows the trajectory traced out by the pad center C over an interval of 2 minutes when $\Omega = 1.05$, $\lambda = 2.81$ radian/second, and

$$A = B = 36,\ R = T = 6,\ S = 36,\ a = 8,\ s = 2 \text{ inches}.$$

This figure illustrates that points on the workpiece within the envelope of the trajectory are well contacted by the tool over a sufficiently long time interval (i.e., there are no 'dead' areas).

In Figure 5 we plot the azimuthal variation of an average material removal rate of a machine having the above settings. The averaging interval is 18 minutes. The near constant values as a function of RI, the distance from the workpiece center, show that this rate is essentially axisymmetric in spite of the fact that there is no overt symmetry in the tool's geometry and motion. Finally, in Figure 6 we plot the radial variation of this rate for different settings of the machine parameter R.

It is clear that useful formulas for Φ (and hence ϕ) depend on the ability to obtain reasonably accurate representations of Preston's constant K^*. This issue has been addressed, for example, in [2], [11], [19-21]. With the cooperation of the Contraves Corporation we

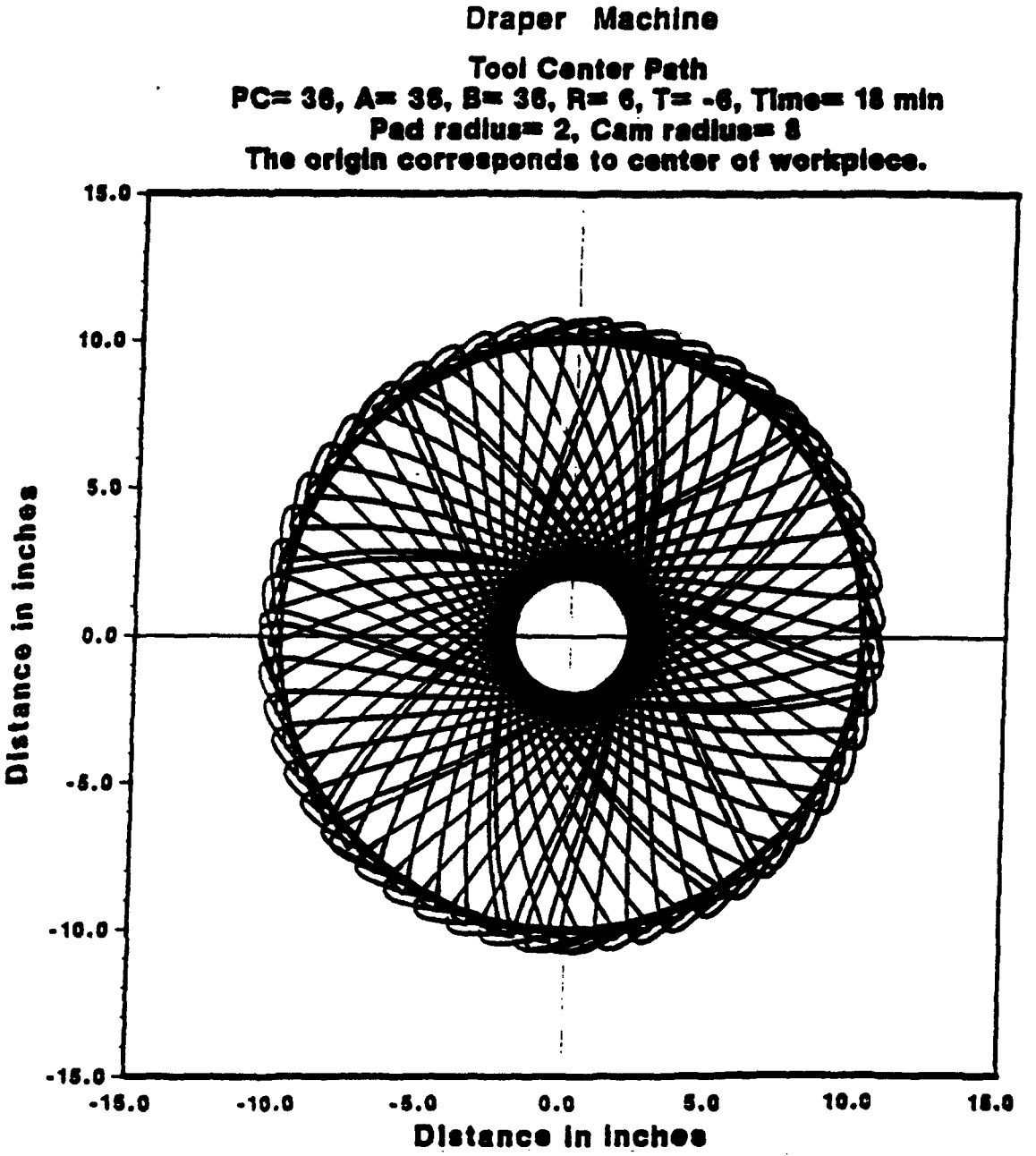

Figure 4. Tool center path for Draper polishing machine.

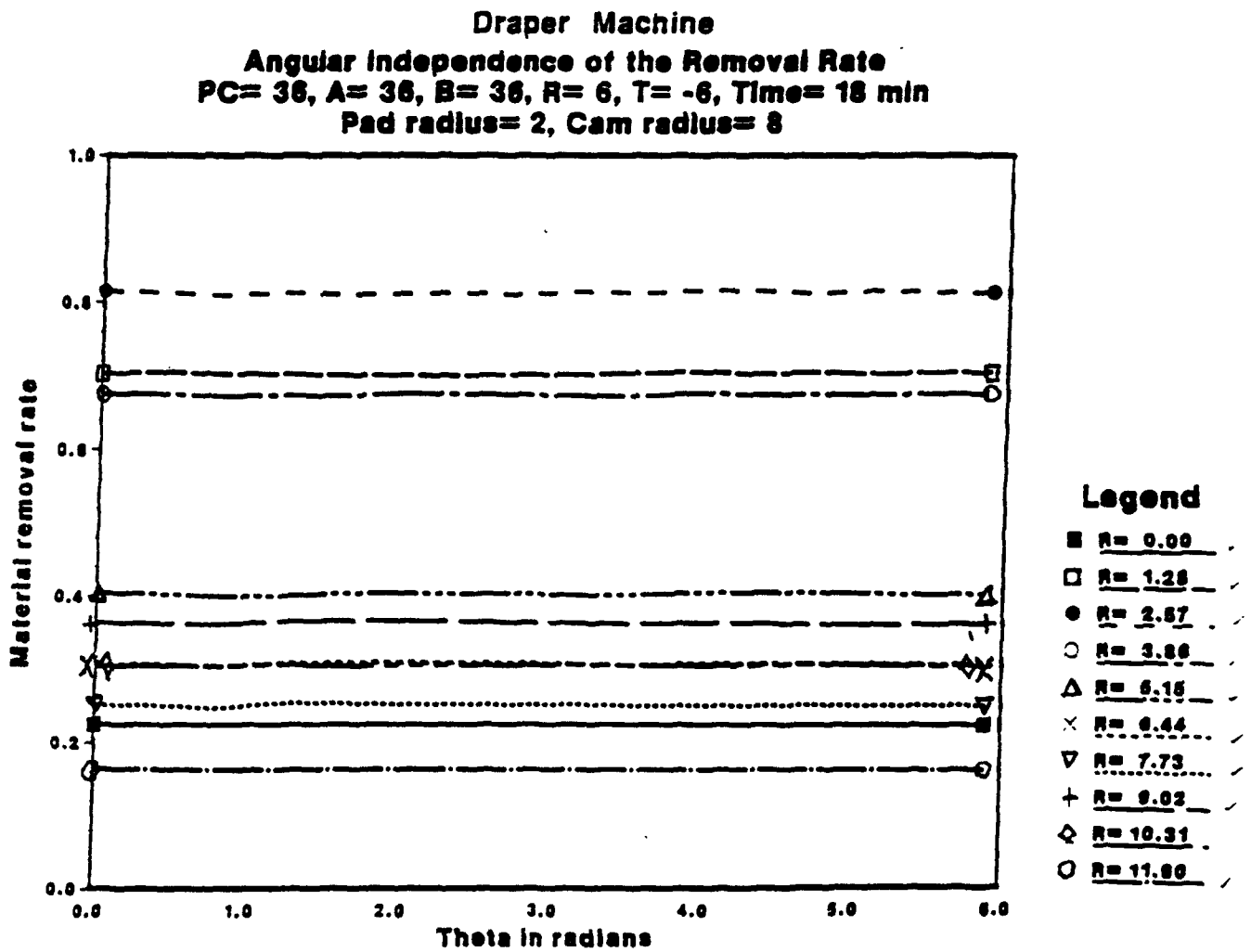

Figure 5. Azimuthal variation of removal profile.

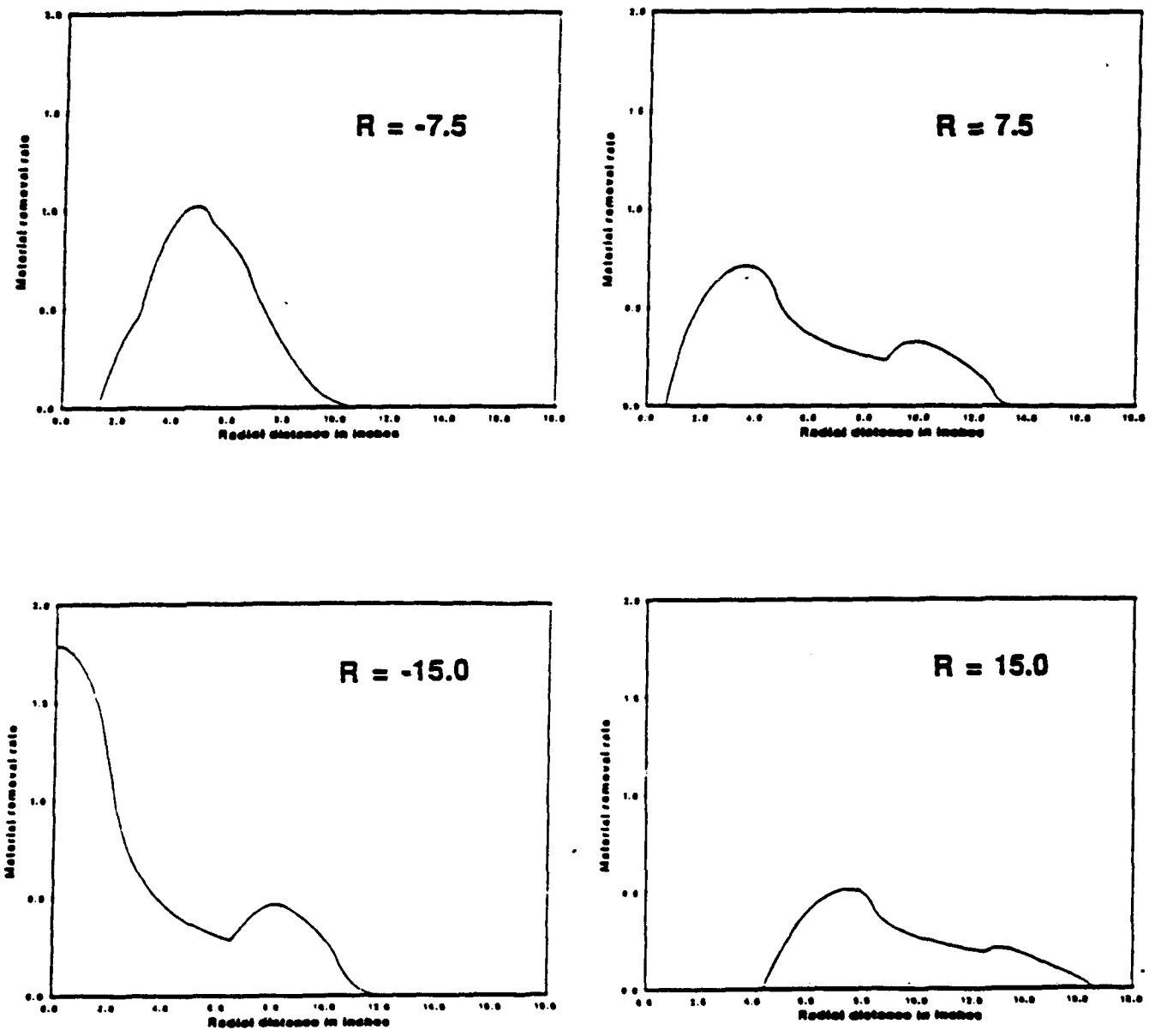

Figure 6. Removal rates for various settings of the parameter. R

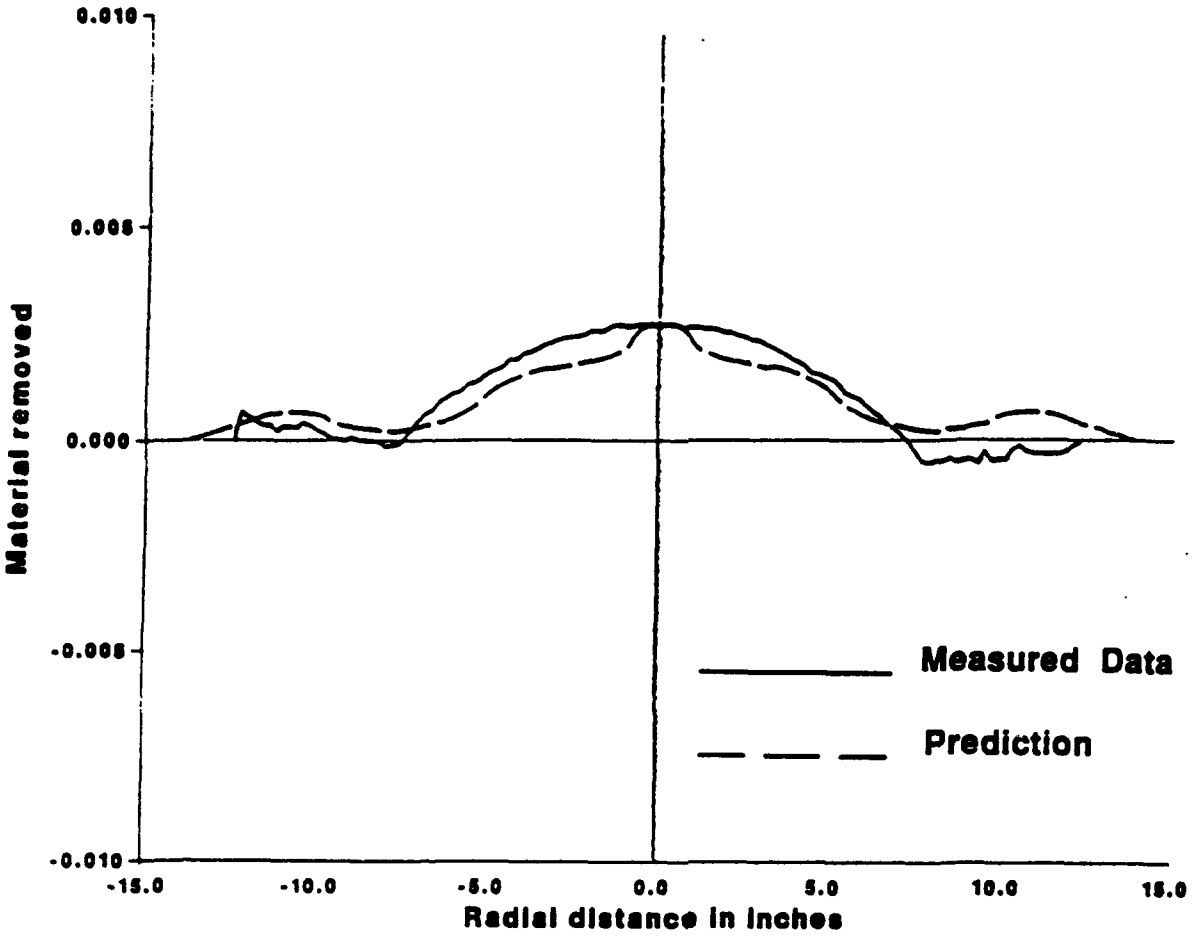

Figure 7. Comparison of Predicted and Experimental Removal Profiles.

have obtained estimates of K^* for various optics. The first task was to validate the shapes of the theoretical removal rates for the Draper polishing machine discussed above. The shop procedure required an optician to record the machine parameters, dwell time, and surface measurements[1] before and after a "rub" of a specific optic. Figure 7 compares the measured material removed from a 12 inch mirror with that predicted by our model. The data used to generate this figure involved two settings of machine parameters and Figure 8 illustrates the theoretical shape of the two removal rates associated with this data. In Figure 7 Preston's constant was estimated so as to match the measured material removed at maximum values in each of two intervals. A least squares fit could also be used for this purpose.

Next we consider the manner in which material is removed from the surface. In view of the definition of the instantaneous removal rate given by (2), it follows that the amount of material removed at point X on the workpiece during the interval $[0, T]$ is simply

$$R(\mathbf{x}) = \int_0^T \Phi(\mathbf{x}, t)dt,$$

[1]Contraves uses a Sheffield Cordax Coordinate Measuring machine equipped with an MP-30/35 processor and computer to obtain the surface measurements.

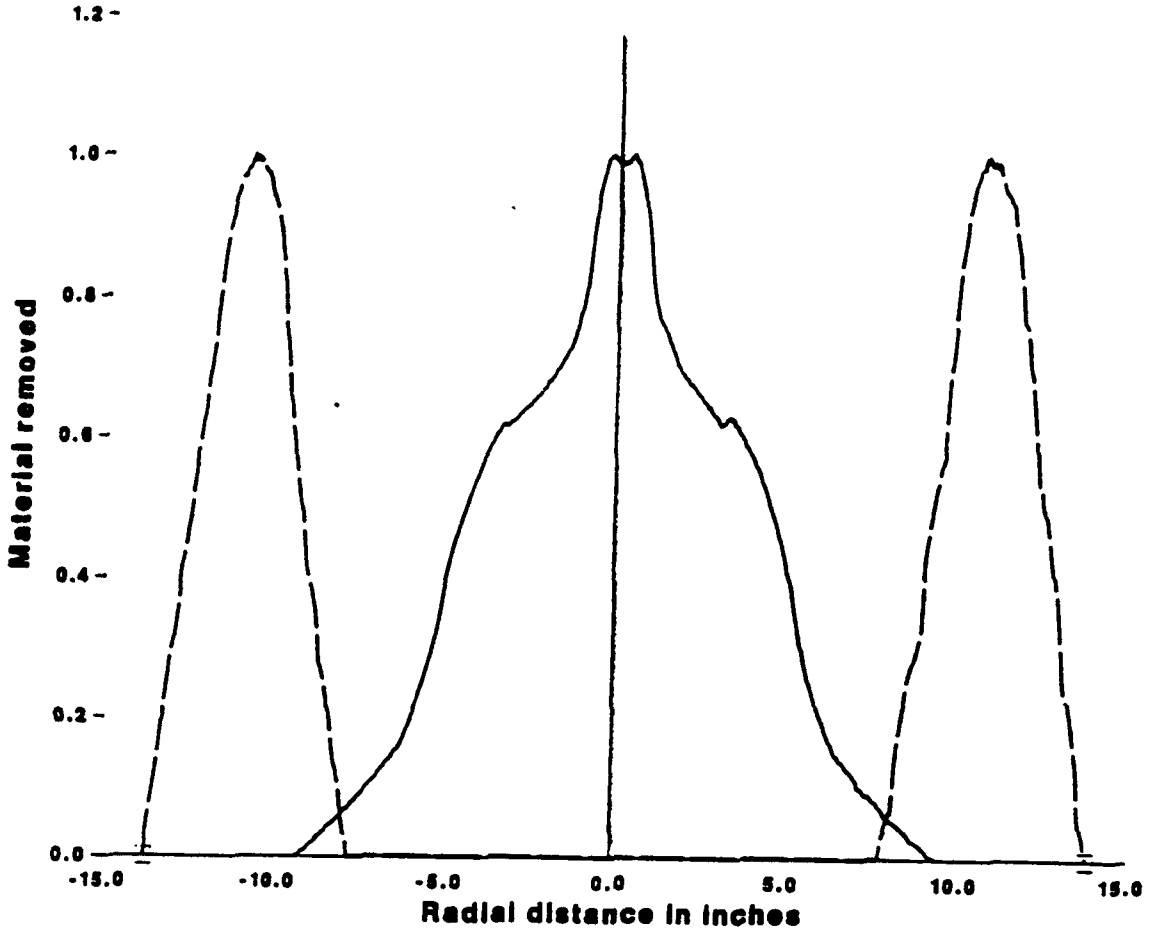

Figure 8. Removal Rates.

where $\mathbf{x}$ is the position vector of X. However, $R(\mathbf{x})$ is of limited value in developing a useful theory of surface finishing. In the first place the removal rate of a specific tool depends on a set of parameters—for example, the Draper tool generates a nine parameter family of material removal rates. These parameters may be regarded as controls by which the finishing process can be adjusted so as to achieve (or approximate) a desired pattern of material removal. Thus in one type of finishing operation a choice of parameters is made and the tool is allowed to run (i.e., dwell on the workpiece surface) for a time interval δt_1. Then the tool is modified by a second choice of parameters and applied for time δt_2. This procedure is repeated, say n times, until the workpiece surface is acceptable.

For such a process, it is natural to define the *machine material removal profile*, i.e., the total amount of material removed by the machine during the process, as

$$S_n(\mathbf{x}) = \sum_{j=1}^{n} \delta t_j \phi_j(\mathbf{x}),$$

where ϕ_j is the average removal rate corresponding to the jth choice of parameters. Note that the functions ϕ_j can in principle be determined once and for all. Consequently, the surface finishing problem reduces to the determination of the *dwell times* δt_j. Several

methods have been suggested to accomplish this, including a simple type of deconvolution [13], as well as L_1 and L_2 optimization [14], [11].

A second type of finishing process that is more aptly termed "computer numerically controlled" utilizes machines that are driven either directly or indirectly by a computer [22]. Typically the workpiece is mounted on a fixed bed and the tool is translated over the workpiece along a path Γ with a speed v provided by the computer. The tool itself is capable of a set of independent motions which we call *local motions*. To model the material removed during such a process, we assume that the workpiece is stationary and the average removal rate ϕ has been developed on the basis of the local motions only. We interpret the reference frame origin O as the *tool center*. The movement of the tool center along Γ constitutes the *global motions*.

To describe the global motions let

$$\mathbf{y}(u) = (y_1(u),\ y_2(u)), \quad a \le u \le b \tag{14}$$

be a parametric representation of the tool center path on the workpiece, and let $v(u)$ be the speed of the tool center at the point $\mathbf{y}(u)$. Then we have shown in [17] that when the speed of the global motions is small compared to that of the local motions, the machine material removal profile, $S(\mathbf{x})$, has the representation

$$S(\mathbf{x}) = \int_a^b \frac{\phi(\mathbf{x} - \mathbf{y}(u))}{v(u)} |\mathbf{y}'(u)| du. \tag{15}$$

The form (15) was derived under the assumption of a given tool center path $\mathbf{y}(u)$ and speed $v(u)$. However, the basic CNC surface finishing problem is to *determine* one (or both) of these quantities so as to make $S(\mathbf{x})$ a good approximation of a given profile.

The fundamental variables in a computer numerically controlled finishing process are the tool head trajectory $\mathbf{y}(u)$, $a \le u \le b$, and speed $v(u)$. Suppose that at each point $\mathbf{x}$ on the workpiece we have a measure of the error profile $f(\mathbf{x})$, i.e., the difference between the desired and existing surface. Then the CNC finishing problem may be stated as follows.

> *Given an error profile $f(\mathbf{x})$ and a tool with associated material removal rate $\phi(\mathbf{y})$, determine a tool center path $\mathbf{y}(u)$ and/or a tool center speed $v(u)$ such that the resulting machine material removal profile $S(\mathbf{x})$, as defined by (15), approximates $f(\mathbf{x})$ to within a desired accuracy.*

In [17] we developed an approach to this problem that exploits the convolution integral form of (15). To describe this approach, let $D_\rho(\mathbf{x}) = \{\mathbf{y} : |\mathbf{y} - \mathbf{x}| \le \rho\}$, and assume that the removal rate $\phi : R^2 \to R$ is a continuous, nonnegative function whose support is contained in the disk $D_{\rho_0}(\mathbf{0})$. Then $H = \min\{\rho :\ \text{supp}\ \phi \subset D_\rho(\mathbf{0})\}$ is well defined and is called the *extent* of the tool. Given a tool with extent H, let

$$C = \int_{-\infty}^{\infty} \int_{-\infty}^{\infty} \phi(\mathbf{y}) d\mathbf{y} > 0.$$

Then the normalized removal rate

$$\phi_H(\mathbf{x}) = \phi(\mathbf{x})/C$$

is called a *mollifier*, and the *mollification* of a given function $f(\mathbf{x})$ that is integrable on R^2 is the convolution integral

$$J_H * f(\mathbf{x}) = \int_{-\infty}^{\infty} \int_{-\infty}^{\infty} J_H(\mathbf{x} - \mathbf{y}) f(\mathbf{y}) d\mathbf{y}.$$

We now relate $J_H * f(\mathbf{x})$ to the removal profile $S(\mathbf{x})$. Assume for simplicity that the workpiece domain W is the rectangle, $0 \leq x_1 \leq a_1$, $0 \leq x_2 \leq a_2$. The generalization to nonrectangular domains is not difficult. Let

$$0 = \xi_0 < \xi_1 < \cdots < \xi_{n-1} < \xi_n = a_1$$

be a partition of the interval $[0, a_1]$ into n equal subintervals of length h, and suppose that we have a quadrature rule such that for $0 \leq y_2 \leq a_2$,

$$\int_0^{a_1} g(y_1, y_2) dy_1 = \sum_{j=0}^{n} w_j g(\xi_j, y_2) + O(h^p).$$

Here the w_j are the weights and p is the order of the rule. If we define the tool head trajectory as the curve

$$\mathbf{y}(u) = (\xi_j, u - j a_2), \quad j a_2 \leq u \leq (j+1) a_2, \quad j = 0, \cdots, n, \tag{16}$$

and if we choose the speed to be

$$v(u) = \frac{C}{w_j f(\xi_j,\ u - j a_2)}, \tag{17}$$

then in [17] it was shown that

$$S(\mathbf{x}) = J_H * f(\mathbf{x}) + O(h^p). \tag{18}$$

In other words, if we apply a strategy that consists of choosing the tool center path according to (16), and the speed according to (17), then the error in replacing the resulting removal rate by the mollification is $O(h^p)$. The curve (16) is simply a set of parallel straight line segments equally spaced across the y_1 coordinate direction of the workpiece.

Although this strategy may not be optimal in the sense of minimizing some norm of the error $S(\mathbf{x}) - f(\mathbf{x})$, it allows for simple error estimates (and attendant controls). For example, suppose that W_0 is a compact subset of W that is at least δ units from the boundary of W. If f is continuous on W, $H \leq \delta$, and L is the order constant in (18), then with the above strategy we have established the error estimate

$$\max_{\mathbf{x} \in W_0} |S(\mathbf{x}) - f(\mathbf{x})| \leq \omega(f; H) + L h^p, \tag{19}$$

where $\omega(f;H) = \max_{|x-y|\leq H} |f(x)-f(y)|$ is the modulus of continuity of f on W. See [17]. If f has continuous first partials on W whose magnitudes are bounded by M, then (19) may be replaced by the more accessible estimate

$$\max_{x\in W_0} |S(x)-f(x)| \leq \sqrt{2}MH + Lh^p.$$

It is clear that in either case the accuracy of the finishing process can be made as precise as necessary by decreasing the control parameters H and h. These theoretical results have been verified by a series of numerical experiments that we reported in [17].

2. Sheet Metal Stamping. A differential-algebraic equation (DAE) is a problem of the form

$$F(x,\dot{x}) = 0, \tag{20}$$

where $F(=F(x,y))$: $\mathbf{R}^n \times \mathbf{R}^n \to \mathbf{R}^n$ satisfies the condition rank $D_y F(x,y) = r < n$ for all $(x,y) \in \mathbf{R}^n \times \mathbf{R}^n$. In particular, equation (20) does not reduce to an explicit ODE via the implicit function theorem. A simple example of DAE is when $x = (x_1, x_2)$ and (20) reads

$$\dot{x}_2 = g_1(x_1,x_2), \quad g_2(x_1x_2) = 0.$$

Thus, the constraint $g_2(x_1,x_2) = 0$ is one of algebraic type, while the first equation is clearly of differential nature.

Despite the growing interest for DAEs in the engineering and numerical literature (see [22-25]) a general existence theory for DAEs was completely lacking. Such a theory was worked out in [27], which is based on the remark that (20) can be reduced to an explicit ODE by a sequence of projections and partial differentiations. This approach should also be helpful for the design of reliable algorithms for the numerical solution of DAEs.

One of the aspects of the approach in [27] which is not completely satisfactory, at least for theoretical purposes, is that it is not intrinsic. In other words, the success of the reduction of the DAE (20) to an explicit ODE may depend upon the choice of the projection. Because of this remark, a different approach, entirely geometric, was developed in [28], where it becomes indispensable to consider, instead of (20), the more general setting of DAEs on manifolds. Then, it can be seen that the iterative procedure discovered in [27] is, in fact, a special case of a general and *intrinsic* process of reduction of a DAE to manifolds of smaller and smaller dimension, until an explicit ODE is obtained. These results, although more theoretical, shed some new light on the problem and completely clarify the definition of the index for a DAE, a terminology used so far in a more intuitive than mathematical sense (except in the linear case).

The important question of the mathematical and numerical characterization of *impasse points* has also been resolved in [29] and [30], respectively. Impasse points are points where solutions of DAEs terminate (that is, cannot be continued further) in *finite* time. They are well-known to play an important role in electrical circuit theory but they may appear in virtually every DAE problem irrespective of its physical origin (chemical reactions, phase transitions, plasticity theory, etc.).

In spite of their acknowledged physical existence, impasse points had so far remained a not fully explained mathematical phenomenon, as they do not occur and have no analog

in explicit differential equations. The clarification of this issue was made possible by combining the aforementioned reduction procedure for DAEs with recent work on *singular* differential equations by Rabier [26].

As a by-product of the better understanding of impasse points (and other higher singularities), sharp connections with some aspects of stiffness in ODEs and convergence questions in singularly perturbed problems have begun to surface. However, much work remains to be done before more precise statements can be made.

The recent theoretical work [26] gives a complete and rigorous analysis of the dynamics in the vicinity of a generic singular point. The results in [26] explain why such deviations from the expected symmetric solution occur, which are due to the slightest breaking of a perfectly symmetric problem. Numerically, such a breaking may be caused by roundoff. More interestingly, since actual problems are never perfectly symmetric. these results show that the true solution may well eventually lose symmetry completely. because the symmetric configuration becomes, loosely speaking, "unstable" beyond the singularity. This demonstrates that enforcing symmetry of the solution by reducing the size of the system, although tempting numerically, is not a safe procedure if a singularity is encountered, for then the calculated solution is no longer significant beyond the singularity. This phenomenon is largely (and probably totally) unknown, and its discovery could have considerable importance in problems in which symmetry of the solution is routinely taken for granted because it is "obvious". From now on, consideration should be given to the nonobvious and unsuspected fact that the slightest breaking of symmetry has drastic effects on the solution in fixed finite time.

Computational experience [34-36] with rate sensitive sheet metal forming problems strongly suggested that the related DAE's in fact possess singularities. There are basically three components to the mathematical formulation of such problems:

(i) the equilibrium equation,

(ii) equations constraining the sheet to follow the punch, and

(iii) the constitutive equations.

The first two lead to nonlinear algebraic equations and the third to a highly nonlinear (stiff) ODE. The (Differential Equation on a Manifold) DEM method [34-36] is based on the observation that the constitutive equations represent a differential equation on a manifold determined by the equilibrium equation and constraint equation. Our problem then is to determine the trajectory of a curve passing through the initial data, lying on the equilibrium manifold and satisfying an ODE (the constitutive equations). This ODE with algebraic constraints is of course a DAE. In [41] we investigated (numerically) the singular behavior of this DAE and its finite element discretization.

The key steps of the DEM approach are:

(i) Introduce finite element approximations to displacements $u_\alpha(\xi,t) \approx \sum_{j=1}^{n} u_{\alpha j}(t)\phi_j(\xi)$, $\alpha = 1,2$; stresses $\tau_\alpha(\xi,t) \approx \sum_{j=1}^{m} \tau_{\alpha j}(t)\eta_j(\xi)$, $\alpha = 1,2$; effective plastic strain, $\bar{\epsilon}(\xi,t) \approx \sum_{j=1}^{m} \bar{\epsilon}_j(t)\eta_j(\xi)$, and normal force $p(\xi,t) \approx \sum_{j=1}^{n} p_j\gamma_j(\xi)$. For this investigation the displacements were approximated by linear elements, the stresses and effective strain by constant elements, and the pressure was approximated by linear elements centered on the

displacement nodes.

(ii) The equilibrium equations and constraint equations lead to $3n$ nonlinear equations

$$\mathbf{F}(\mathbf{Y}, t) = 0 \tag{21}$$

in the $(6n-3)$ variables $\mathbf{Y} = (\mathbf{T}_1, \mathbf{T}_2, \mathbf{E}, \mathbf{U}_1, \mathbf{U}_2, \mathbf{P})^T$ where $\mathbf{U}_{ai} = u_{ai}, \mathbf{T}_{aj} = \tau_{aj}, \mathbf{E}_j = \bar{\epsilon}_j$ and $\mathbf{P}_j = p_j$.

(iii) Approximation of the constitutive equation by collocation at the $m = n-1$ stress nodes yields a differential equation

$$B(\mathbf{Y})\dot{\mathbf{Y}} = \mathbf{G}(\mathbf{Y}, t) \tag{22}$$

where the matrix B is $(3n-3) \times (6n-3)$.

(iv) The ODE (22) is solved on the $(3n-2)$–dimensional *equilibrium manifold* consisting of all solutions of (21). This can be accomplished using software packages such as LSODI [38] or DASSL [39]. In this investigation, the software package LSODI was used to integrate (22) subject to (21). We note that equations (21) and (22) together form a DAE.

The basic geometry is shown in Figure 9 for a flat bottomed punch. The sheet is assumed initially flat and is stretched over a die by a punch. We assume a state of plane strain; the component of strain in the direction perpendicular to the paper is zero. Points on the material are identified by their initial distance ξ from the z–axis. The sheet initially lies in $\xi_L \leq \xi \leq \xi_R$. In Figure 9, $\xi_L = 0.0$ and $\xi_R = 100.0$ mm. The current *horizontal* and *vertical displacements* are u_1 and u_2, respectively, and are functions of ξ and time t.

The *principal logarithmic strain components* are

$$\epsilon_1 = \ln\left[\left(1 + \frac{\partial u_1}{\partial \xi}\right)^2 + \left(\frac{\partial u_2}{\partial \xi}\right)^2\right]^{1/2}$$
$$\epsilon_2 = 0$$

where for the strains and stresses subscript 1 is tangential to the sheet (ξ–direction) and 2 is normal to the paper.

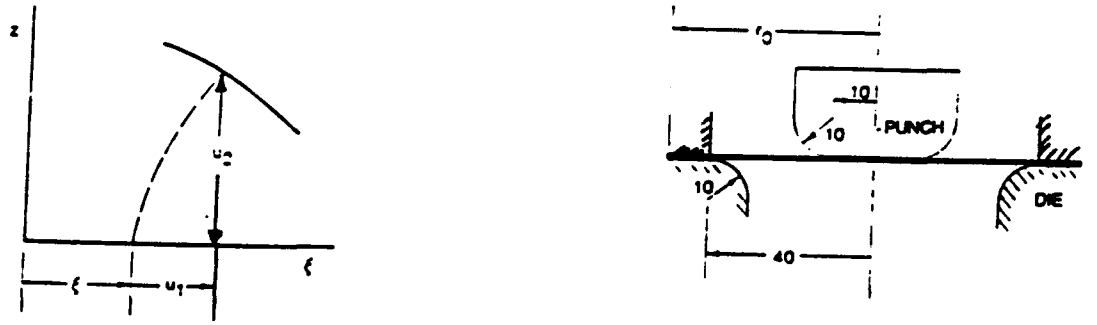

Figure 9. Punch geometry.

The problem has a natural symmetry with respect to the centerline of the punch, and the chosen finite element discretization agrees with this symmetry. It must then be expected that the solution of the discrete system (21) - (22) exhibits the same symmetry at each time $t > 0$. Thus, aside from the problem corresponding to the entire sheet [0.0, 100.0] (Problem F, for "full") it makes sense to consider the problem corresponding to, say, the right part of the sheet [50.0, 100.0] (Problem H, for "half") where symmetry is enforced by the condition

$$u_1(50.0, t) = 0, \quad u_2(50.0, t) = \lambda t. \tag{23}$$

The surprising fact now is that it was observed some time ago by the authors of [34-36] that the solution to the "full" Problem F *eventually loses symmetry* and in particular no longer satisfies the condition $u_1(50.0, t) = 0$ for increasing values of t. Instead, rather large (and sometimes oscillating in sign) values were obtained for $u_1(50.0, t)$. Although this phenomenon was partly controlled through judicious choices of error tolerances and steplengths in LSODI, it appeared to be impossible to eliminate. Furthermore, the steplength and tolerance adjustments needed to preserve symmetry for as long a time as possible were found to be extremely sensitive to parameter values (velocity λ of the punch, coefficient of friction, etc. ...) and hence could not be specified once and for all for an entire range of parameter values. This sudden lack of robustness in the DEM solution procedure was to say the least disquieting, and could not be related to any of the usual causes of numerical instabilities. In fact, no concomitant operational difficulty was detected either: the solution was calculated with no apparent trouble, only loosing its expected symmetry after at most 25 to 30 seconds.

A third problem (Problem S, for "symmetrized", was also considered, that enforces symmetry by averaging the solution of Problem F at each step instead of using the constraints (23). This problem can be viewed as an intermediate between Problems F and H and will be used for various comparisons.

Figure 10 illustrates the centerline horizontal displacement $u_1(50, t)$ for Problem F and three choices of mesh refinement. Sample numerical evaluations are given in Table 1. For example, in the case of $n = 21$ (20 elements) the centerline displacement at $t = 40.0$ secs. is $u_1(50, 40.0) = -13.04$ mm. For these calculations the maximum step size was taken to be 1.0 sec, the maximum error tolerance was 0.5×10^{-2}, and the backward Euler method was used for time integration.

	$t = 10.0$	$t = 20.0$	$t = 25.0$	$t = 30.0$	$t = 35.0$	$t = 40.0$
$n = 21$	$-3.7E-3$	$-1.3E-2$	$1.7E-2$	-3.03	-8.02	-13.04
$n = 31$	$6.1E-4$	$9.6E-3$	$5.5E-1$	2.95	7.13	13.10
$n = 41$	$1.1E-4$	$1.5E-4$	$-1.0E-3$	-0.14	-4.34	-9.73

Table 1. Centerline displacement $u_1(50, t)$ for Problem F.

In order to assess the effect of error tolerances (ER) and maximum steplength (SL) on the centerline displacements, various combinations were considered. Some of these results are presented in Figure 11. The conclusions are the same; eventually the solution fails to be symmetric, the deviation from symmetry may be of either sign and its magnitude

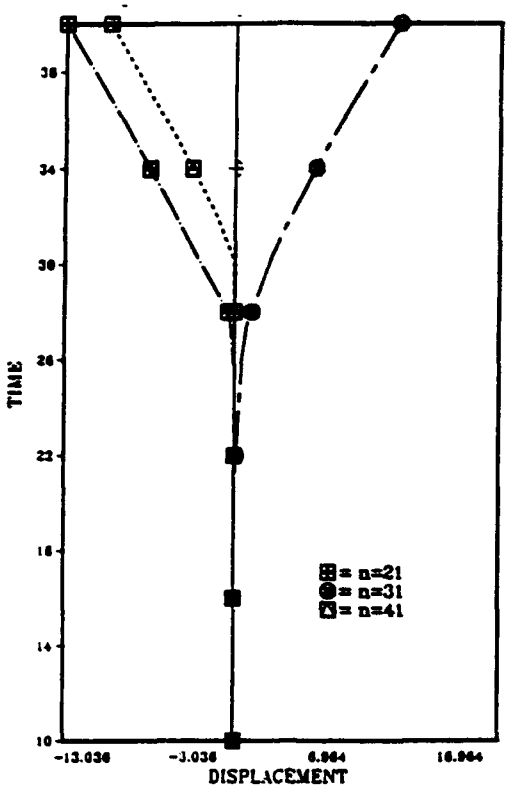

Figure 10. Centerline displacement for Problem F varying mesh size only.

increases several orders of magnitude in the time interval $(25.0, 30.0)$. This numerical experimentation suggests that small perturbations (of the *order of magnitude* of computer roundoff errors) in the computed solution cause the integrator (LSODI) to accept points on neighboring trajectories which ultimately evolve into *non-symmetric* solutions with centerline horizontal displacements that are roughly the magnitude of the punch radius. As we shall see, this behavior can be related to the existence of singularities for the system (21) - (22).

Figure 12 contains plots of the strain $\epsilon_1(\xi, 30)$ for Problem F, Problem S and Problem H. For Problem H, the solution is reflected about the line $\xi = 0$. Note that the solution of the (full region) Problem F produces strains which, compared with the values obtained for Problem H, are gross overestimates for a portion of the punch contact region and gross underestimates for another portion.

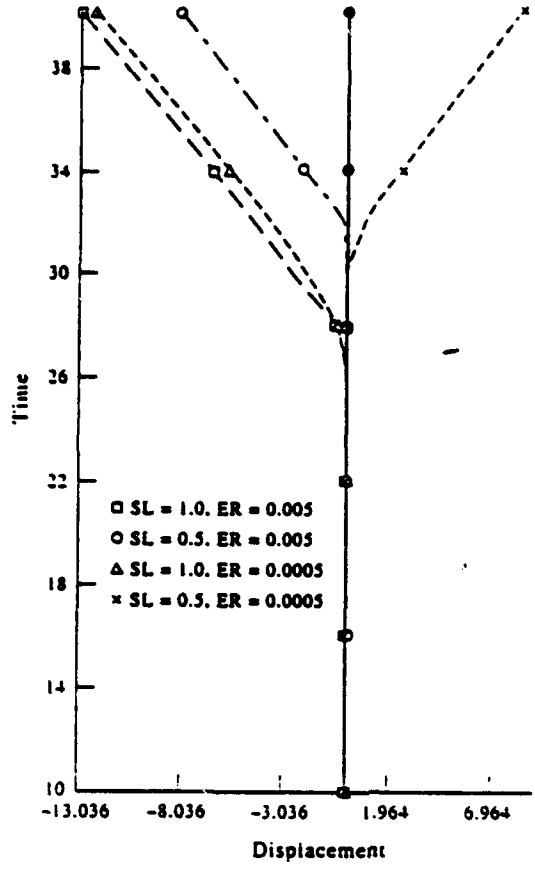

Figure 11. Centerline displacement for Problem F varying maximum steplength (SL) and error tolerance (ER), with a fixed mesh ($n = 21$).

To experiment further, we tested the hypothesis that small perturbations in the initial data will yield only small perturbations in the solution for all finite time. This is a property one should certainly expect under usual circumstances. The initial condition $u_1(\xi, 0) = 0$ was modified so that $u_1(50, t) = \delta$ for various values of the parameter δ (see Figure 13). As illustrated, it turns out that small perturbations in the initial data cause very large deviations from symmetry even for relatively small values of time (or punch depth). Similar results were obtained for $n = 21$ (20 elements). Early attempts (for example, [40]), to apply the finite element method to punch stretching involved a *rate form* of the equilibrium equations. Such a form results from (21) by time differentiation as

$$\mathbf{F}_{\mathbf{Y}_1}(\mathbf{Y}, t)\dot{\mathbf{Y}}_1 + \mathbf{F}_{\mathbf{Y}_2}(\mathbf{Y}, t)\dot{\mathbf{Y}}_2 = -\mathbf{F}(\mathbf{Y}, t) \tag{24}$$

where $\mathbf{Y}_1 = (\mathbf{T}_1, \mathbf{T}_2, \mathbf{E})^T$ and $\mathbf{Y}_2 = (\mathbf{U}_1, \mathbf{U}_2, \mathbf{P})^T$.

Because the matrix $\mathbf{B}$ in (22) has the form $(\mathbf{I}, \mathbf{B}_2)$ the discrete constitutive equations (22) can be rewritten as

$$\dot{\mathbf{Y}}_1 + \mathbf{B}_2(\mathbf{Y}_2)\dot{\mathbf{Y}}_2 = \mathbf{G}(\mathbf{Y}, t). \tag{25}$$

Hence, combining (24) and (25) we have

$$\begin{pmatrix} I & B_1(\mathbf{Y}_2) \\ \mathbf{F}_{\mathbf{Y}_1}(\mathbf{Y},t) & \mathbf{F}_{\mathbf{Y}_2}(\mathbf{Y},t) \end{pmatrix} \begin{pmatrix} \dot{\mathbf{Y}}_1 \\ \dot{\mathbf{Y}}_2 \end{pmatrix} = \begin{pmatrix} \mathbf{G}(\mathbf{Y},t) \\ -\mathbf{F}_t(\mathbf{Y},t) \end{pmatrix}. \tag{26}$$

Any solution of the ODE (26) satisfying the initial condition is also a solution of the DAE (21)-(22).

We now investigate the ODE (26) which, for simplicity of notation. we shall rewrite in the form

$$\mathbf{A}(\mathbf{Y},t)\dot{Y} = \mathbf{H}(\mathbf{Y},t), \tag{27}$$

where

$$A(\mathbf{Y},t) = \begin{pmatrix} I & B_2(Y_2) \\ \mathbf{F}_{Y_1}(\mathbf{Y},t) & \mathbf{F}_{Y_2}(\mathbf{Y},t) \end{pmatrix}, \tag{28}$$

$$\mathbf{H}(\mathbf{Y},t) = \begin{pmatrix} \mathbf{G}(\mathbf{Y},t) \\ -\mathbf{F}_t(\mathbf{Y},t) \end{pmatrix}. \tag{29}$$

First and foremost, it must be recalled that the standard existence and uniqueness theory for ODE's applies only when $\mathbf{A}(\mathbf{Y},t)$ is invertible, i.e. (27) is equivalent to the explicit equation $\dot{Y} = \mathbf{A}(\mathbf{Y},t)^{-1}\mathbf{H}(\mathbf{Y},t)$. The mathematical study of the case where $\mathbf{A}(\mathbf{Y},t)$ becomes singular has been developed only quite recently. We report only the features that appear to be relevant to the problem of interest and we refer to the paper [26] for further details. One crucial and nonevident fact is that singularities need not only affect trajectories on which they lie. As it turns out, some singularities may affect the entire flow, precisely by *deviating* trajectories from their "expected" course. This does not require the deviated trajectories to contain any singular point, nor even to ever get close to them.

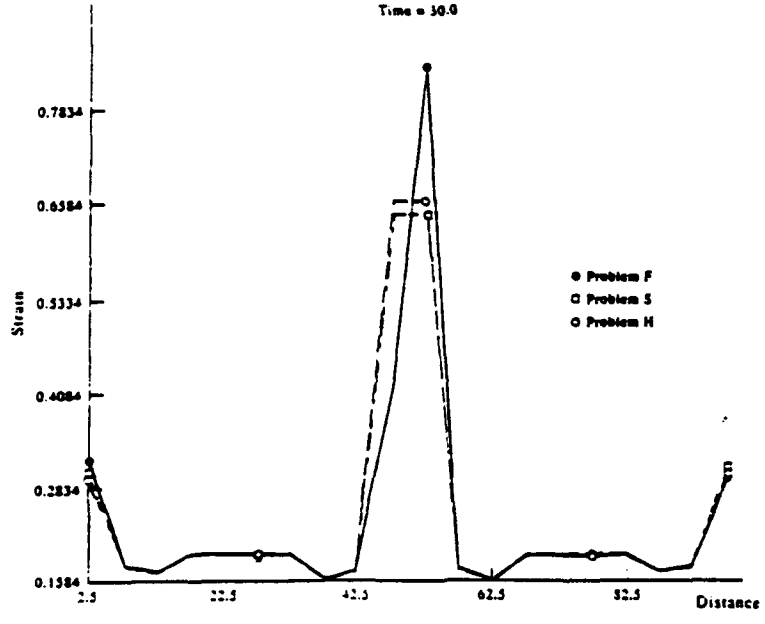

Figure 12. Comparison of strain ϵ_1 for different problems.

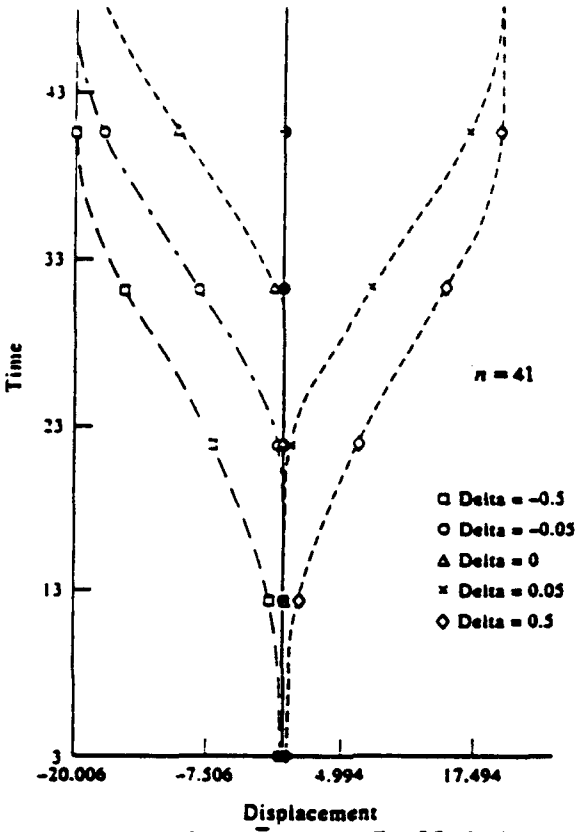

Figure 13. Centerline displacement for Problem F perturbing the initial condition.

For the system (26), the most commonly encountered kind of singularity is the so–called "standard singular point" where exactly two solutions terminate (accessible standard singular point) or emanate (inaccessible standard singular point) at a given time t_*. The terminology "accessible" and "inaccessible" is meant to emphasize that the standard singular point, say Y_*, is actually met by trajectories initiating at $t < t_*$ (accessible case) or cannot be met by any such trajectory (inaccessible case: note that since the only solutions near Y_* emanate from Y_* at time t_*, *no* solution starting *anywhere* at time $t < t_*$ will ever go through Y_* at time t_* or other). In addition, standard singular points are not isolated. Rather, they occur in hypersurfaces that therefore separate the space (locally at least) in two regions. Hypersurfaces of accessible standard singular points thus represent "walls" beyond which solutions cannot be extended and hence can be viewed as catastrophes. Hypersurfaces of inaccessible standard singular points have a different but equally strong effect on solutions: since these hypersurfaces consist of points that cannot be reached in increasing time, all the solutions going toward them eventually have to *bounce* and continue in a different, unanticipated direction.

The numerical results that we present in [41] tend to corroborate the thesis that the deviations from symmetry numerically observed for Problem F are due to singularities: although the mathematical solution of (26) corresponding to symmetric initial data is symmetric for all times, slight imperfections (roundoff) originally destroy this symmetry, and next the system evolves as one of the bouncing trajectories. We shall see that despite that no singularity is detected on the solution curves of the system (26), such singularities are found in their close vicinity. In fact, our results indicate that the trajectories of the system (26) get closer and closer to the hypersurface of singular points as time elapses. Earlier, we have mentioned roundoff to be the reason why perfect mathematical symmetry

is initially broken. But the singularities are responsible for making "visible" in finite time this initially negligible perturbation because they induce an ***extreme sensitivity upon initial conditions*** (quite comparable, although very different in its nature, to loss of stability in static problems). But then, it must be expected that *any* breaking of the mathematical symmetry, due to roundoff or other error, will result in a trajectory that deviates in finite time and by a finite (as opposed to infinitesimal) amount from the symmetric solution. This means that eventually the latter cannot be considered a reasonable solution for any problem that differs, no matter how little, from the mathematically symmetric one. In other words, while it is *apparently* harmless to neglect the slight imperfections that destroy symmetry in a nearly symmetric problem, the truth may be quite different. Indeed, accepting the symmetric configuration as a reasonable approximation leads to accepting its symmetric solution as being sufficiently close to the correct one while in fact the true solution is a significantly different, deviated one. This is fully corroborated by the results summarized in Figure 13 and already discussed earlier. Naturally, the value of this conclusion depends upon the accuracy of the model, but we note that it is potentially valid in any model exhibiting singularities (on the other hand, examples show that not every type of singularity deviates trajectories, so that other phenomena are possible).

In [41], we establish the existence of singularities for the matrix $\mathbf{A}(\mathbf{Y},t)$ involved in the ODE (26) and show that the solutions of (26) get closer and closer to singular points of $\mathbf{A}$ as time increases. It can be shown [41] that

$$\det A = \det(\mathbf{F}_{\mathbf{Y}_2} - \mathbf{F}_{\mathbf{Y}_1}\mathbf{B}_2) \tag{30}$$

where the matrix $\mathbf{T} \equiv \mathbf{F}_{\mathbf{Y}_2} - \mathbf{F}_{\mathbf{Y}_1}B_1$ is $3n$ by $3n$. Hence, the characterization of any singular behavior of the ODE (26) reduces to investigating the spectrum of the smaller matrix $\mathbf{T}(\mathbf{Y},t)$.

The software package EISPAK was used to calculate the spectrum of the matrix $\mathbf{T}(\mathbf{Y},t)$ and the eigenvalue of minimum modulus was determined as a function of time. Figure 14 contains plots of this minimum eigenvalue for Problem S and Problem H with maximum steplengths of 1 sec and 0.5 sec. Note that for the smaller steplength the symmetrized full region problem (Problem S) produces a singular matrix $\mathbf{T}(\mathbf{Y},t)$ for t near 140 secs. While the other cases do not become singular, we do note that the minimum eigenvalue is tending to zero for large time values. (See Figure 15 for $n = 41$ nodes).

For the cases presented here and for all cases investigated, the plots of minimum eigenvalue versus time start off close to zero (reflecting the singularity in the solution at $t = 0$, [41]. The eigenvalue then increases, peaks between 25.0 and 30.0 seconds and the decreases over time to zero or near zero. It was suggested[2] that the maximum may occur when unloading begins. Figure 16 verifies this conjecture. The minimum eigenvalue reaches its maximum when the load $\sigma \equiv \tau_1 h_0 e^{-\epsilon_1}$ attains its maximum as a function of strain ϵ_1. To assess if singular points exist close to the solution curve the following experiment was performed. Let $\mathbf{Y}^k$ be the solution at the kth time step and define Δ^k to be a vector of the same dimension $(6n-3)$ defined as follows. If node i is not in contact with the die or

[2]M. Wenner, private communication.

punch and $Y_{i_j}, j = 1, 2, \cdots, 6$ are the six entries associated with node i, then define

$$\Delta_{i_j}^k = -(Y_{i_{j+1}}^k - Y_{i_{j+1}}^{k-1}), \quad \Delta_{i_{j+1}}^k = (Y_{i_j}^k - Y_{i_j}^{k-1}), \ j = 1, 3, 5.$$

Otherwise

$$\Delta_i^k = 0.$$

Then Δ^k is orthogonal to $Y^k - Y^{k-1}$. We choose as a point "close" to the solution curve $Y(t)$, the point

$$Z^k = Y^k + \delta \Delta^k$$

and vary the parameter δ. For $t = 10.0$ and $t = 40.0$ (as with all other cases considered) the matrix $T(Z^k)$ is singular for relatively small values of δ. That is, apparently the coefficient matrix in the ODE (26) is very close (as a function of Y) to being singular for all time t. (See Figure 17).

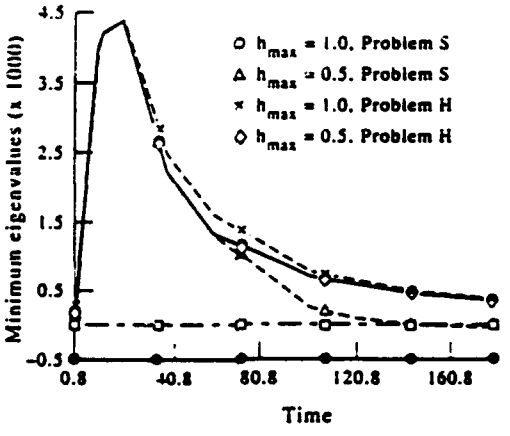

Figure 14. Minimum eigenvalue of $T(Y, t)$, 21 *nodes.*

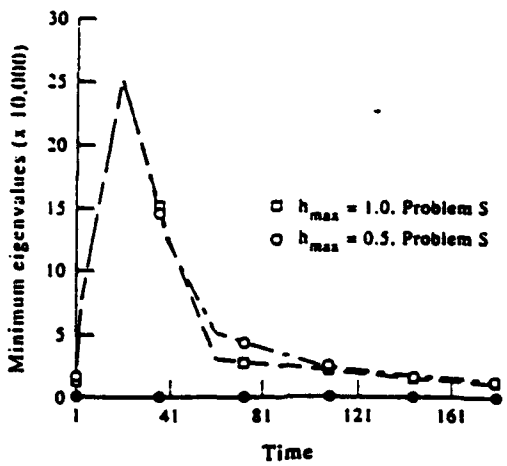

Figure 15. Minimum eigenvalue of $\mathbf{T}(\mathbf{Y}, t)$, 41 *nodes.*

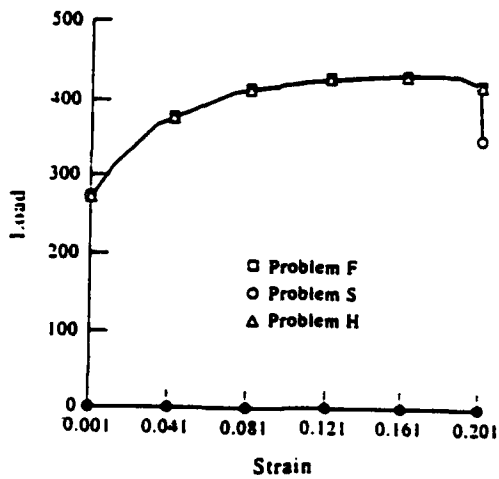

Figure 16. Load versus strain, 41 *nodes.*

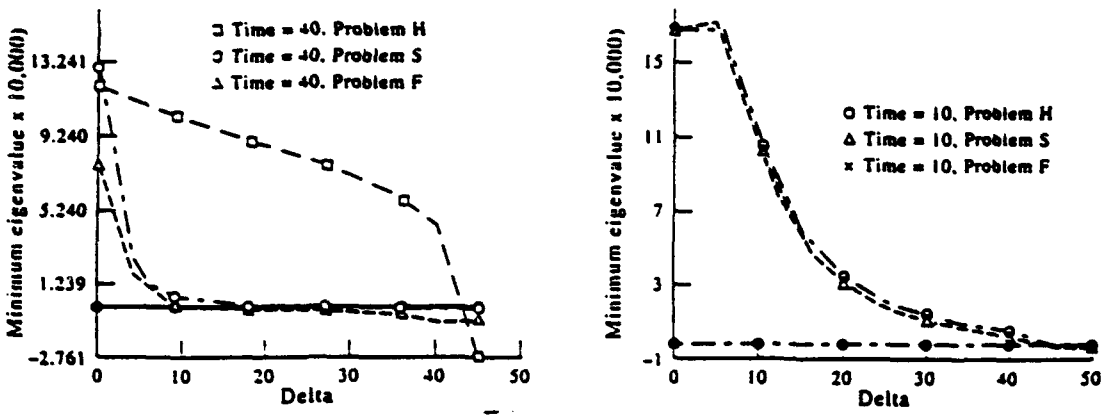

Figure 17. Minimum eigenvalue of $T(\mathbf{Z}^k)$.

General Note

Some of the mathematical tools involved in the preparation of [27-30] and other related ideas have been used in more theoretical works by Rabier [31-33] and therefore partial support from AFOSR 90-0094 has been acknowledged in these papers. The article [31] is relevant in general nonlinear (PDE type) problems. It shares with [27] the feature of making crucial use of vector bundles. Stability questions involved in the treatment of higher singularities of DAEs originally motivated [32], and the abstract algebraic concepts developed in [33] stemmed directly from the study of symmetry breaking in bifurcation problems. These results could (although this is not certain as yet) have great significance in the analysis of DAEs involving symmetry, that physical examples already seems to justify.

References

1. R. Aspden, et. al., *Computer Assisted Optical Surfacing*, Appl. Opt. **11** (1972), 2739–2747.
2. K.B. Paxton, et.al., *Uniform Polishing of Convex Aspheres with an Elastic Lap*, Appl. Opt. **14** (1975), 2274–2279.
3. D.J. Bajuk, *Computer Controlled Generation of Rotationally Symmetric Aspheric Surfaces*, Optical. Eng. **15** (1976), 401–406.
4. R.A. Jones, *Fabrication of Small Nonsymmetrical Aspheric Surfaces*, Appl. Opt. **18** (1979), 1244–1246.
5. ———, *Optimization of Computer Controlled Polishing*, Appl. Opt. **16** (1977), 218–2247.
6. A.H. Greenleaf, *Computer-controlled Optical Surfacing*, Proc. SPIE 228, Act. Opt. Devices and Appl. (1980), 41–54.
7. R.A. Jones, *Computer Controlled Polisher Demonstration*, Appl. Opt. **19** (1980), 2072–2076.
8. ———, *Computer-controlled Grinding of Optical Surfaces*, Appl. Opt. **21** (1982), 874–877.
9. ———, *Computer-controlled Polishing of Telescope Mirror Segments*, Optical. Eng. **22** (1983), 236–240.
10. ———, *Computer-controlled Optical Surfacing with Orbital Tool Motion*, Optical. Eng. **25** (1986), 785–790.
11. R.E. Wagner and R.R. Shannon, *Fabrication of Aspherics Using a Mathematical Model for Material Removal*, Appl. Opt. **12** (1974), 1683–1689.
12. D.J. Wenzel and D.S. McFalls, *An Optimal Material Removal Strategy for Automated Repair of Aircraft Canopies*, Proc. IEEE Int. Conf. on Robotics and Automation, Scottsdale, Ariz. (1989), 370–376.
13. N.J. Brown, *Computationally Directed Axisymmetric Aspheric Figuring*, Opt. Eng. **17** (1978), 602–620.
14. C.A. Hall and T.A. Porsching, *Approximation Methods in the Numerically Controlled Fabrication of Optical Surfaces. Part I: Finite Dimensional Material Removal Profile Spaces*, IMA J. Numer. Anal. **12** (1992), 67–84.
15. ———, *Approximation Methods in the Computer Numerically Controlled Fabrication of Optical Surfaces. Part II: Mollifications*, IMA J. Numer. Anal. **12** (1992), 259–269.
16. ———, *Approximation Methods and the Computer Numerically Controlled Fabrication of Optical Surfaces*, Advanced Optical Manufacturing and Testing II, Proc. SPIE **1531** (1992), 205–215.
17. T.A. Porsching, C.A. Hall, T.L. Bennett and J. M. Ernsthausen, *A Mathematical Model of Material Removal with Application to CNC Finishing*, Math. Comp. Modelling **18** (1993), 25–40.
18. F.W. Preston, *The Theory and Design of Plate Glass Polishing Machines*, J. Soc. Glass Tech. **11** (1927), 214–256.
19. L.H. Meuser, *Comparative Grinding Characteristics of Selected Long-Wavelength Infrared Materials*, Program Opt. Soc. Am., Tucson Ariz. **10** (1971).

20. W. Rupp, *Loose Abrasive Grinding of Optical Surfaces*, Appl. Opt. **11** (1972), 2797–2810.
21. G.E. Wiese and R.E. Wagner, *Physical Model for Predicting Grinding Rates*, Appl. Opt. **13** (1974), 2719–2722.
22. D. Gibbs and T.M. Crandell, *An Introduction to CNC Machining and Programming*, Industrial Press, New York, 1991.
23. Brenan, K. E., Campbell, S. L. and Petzold, L. R., *Numerical solution of initial-value problems in differential-algebraic equations*, North-Holland, 1989.
24. Griepentrog, E. and Maerz, R.,, *Differential-algebraic equations and their numerical treatment*, Teubner, 1986.
25. Hall, C. A., DeCarlo, L. E., Wenner, M. L., Troyani, N. L., *Elastic-viscoplastic DEM modeling of in-plane stretching of sheet metal*, Int. J. Num. Meth. Eng. **36** (1993), 3617–3627.
26. Rabier, P. J., *Implicit differential equations near a singular point*, J. Math. Anal. Appl. **144** (1989), 4225–449.
27. Rabier, P. J. and Rheinboldt, W. C., *A general existence and uniqueness theory for implicit differential-algebraic equations*, Diff. Int. Eqs. **4** (1991), 563–582.
28. Rabier, P. J. and Rheinboldt, W. C., *A geometric treatment of implicit differential-algebraic equations*, J. Diff Eqs. (to appear).
29. Rabier, P. J. and Rheinboldt, W. C., *On impasse points of differential algebraic equations*, J. Math. Anal. Appl. **18** (1994), 429–454.
30. Rabier, P. J. and Rheinboldt, W. C., *On the computation of impasse points of quasilinear differential - algebraic equations*, Math. Comp. **62** (1994), 133–154.
31. Fitzpatrick, P. M., Pejsachowicz, J. and Rabier, P. J., *The degree of Csup2 proper Fredholm mappings I*, J. reine ang. Math. **427** (1992), 1–33.
32. Rabier, P. J., *On global diffeomorphisms of euclidian space*, Nonlinear Analysis, TMA **21** (1993), 925–947.
33. Rabier, P. J., *Intrinsic isotropy subgroups of finite groups*, J. Algebra **154** (1993), 108–124.
34. Cavendish, J.C., Wenner, M.L., Burkhardt, J., Hall, C.A. and Rheinboldt, W.C., *DEM: a new computational approach to sheet forming problems*, Int. J. Numer. Meth. Eng. **23** (1986), 847–862.
35. Cavendish, J.C., Wenner, M.L., Burkhardt, J., Hall, C.A. and Rheinboldt, W.C., *Punching stretching of sheet metal and differential equations on manifolds*, Int. J. Numer. Meth. Eng. **25** (1988), 269–282.
36. Hall, C.A., Rheinboldt, W.C., and Wenner, M.L., *Differential equations on a manifold (DEM) formulation of metal forming*, NUMIFORM 89, Proc. of Int. Conf. on Industrial Forming Processes, Balkema Publishers, 1989.
37. Birkhoff G. and Rota, G.C., *Ordinary differential equations, Second edition*, John Wiley & Sons, New York, 1969.
38. Hindmarsh, A.C., *ODE solves for time dependent PDE software*, Presented at IFIP PDE software conference, Sokerkoping, Sweden, August, 1983, available in preprint form as UCRL 89311, Lawrence Livermore National Laboratory..
39. Petzold, L.R., *A description of DASSL: A differential/algebraic system solver*, Proc. of IMACS World Congress, Montreal, Canada, August (1982).
40. Wang, N.M. and Wenner, M.L., *Elastic-viscoplastic analysis of simple stretch forming problems*, Proc. General Motors Research Laboratories Symposium, Plenum Press, New York, 1978.
41. Hall, C.A., Lei, X. and Rabier, P.J., *A Nonstandard Symmetry Breaking Phenomenon in Sheet Metal Stretching*, Int. J. Eng. Sci. (to appear).